Mathematical Modeling of Coolant Flow in Discontinuous Drilling Processes with Temperature Coupling

Michael Fast[1,*]**, Otto Mierka**[1]**, Stefan Turek**[1]**, Tobias Wolf**[2]**,** and **Dirk Biermann**[2]

[1] Technische Universität Dortmund, Fakultät für Mathematik, Lehrstuhl LSIII, Vogelpothsweg 87, 44227 Dortmund

[2] Institut für Spanende Fertigung, Technische Universität Dortmund, Baroper Str. 303, 44227 Dortmund

Nickel-based alloys, like Inconel 718, are widely used in industrial applications due to their high-temperature strength and high toughness. However, machining such alloys is a challenging task because of high thermal loads at the cutting edge and thus extensive tool wear is expected. Consequently, the development of new process strategies is needed. We will consider the discontinuous drilling process with coolant. The main idea is to interrupt the drilling process in order to let the coolant to flow around the cutting edge and to reduce thermal loads. Since measurements inside the borehole are (nearly) impossible, simulations are a key tool to analyze and understand the proposed process.

In this paper, a 3D fluid flow simulation model with Q2P1 Finite Elements in combination with the Fictitious Boundary Method is presented to simulate the coolant flow around the drill inside the borehole. The underlying equations are transformed into a rotational frame of reference overcoming the challenges of mesh design for high rotational domains inside the fluid domain. Special treatment of Coriolis forces is developed, that modifies the 'Pressure Poisson' Problem in the projection step improving the solver for high angular velocities. To further take high velocities into account, a two-scale artificial diffusion technique is introduced to stabilize the simulation. Finally, Q1 Finite Elements are used to simulate the heating and cooling processes in both the tool and the coolant during the complete discontinuous drilling process. The simulation is split into a 'contact' and a 'no contact' phase and a coupling strategy between these phases is developed. FBM is utilized to switch between the two configurations, thus only one unified grid for both configurations is needed. The results are used to gain insight into the discontinuous drilling process and to optimize the process design.

1 Introduction

The Nickel based alloy Inconel 718 is a widely used material for high-temperature applications. Inconel 718 is characterized by high temperature strength and low thermal conductivity which makes it a suitable alloy for turbine blades, exhaust gas components, and turbochargers. However, because of these beneficial properties, machining of Inconel 718 is a challenging task from an engineering standpoint. Due to the high temperature strength, excessive thermal loads on the tool are to be expected leading to extensive tool wear or breakage. Consequently, the use of coolant is necessary. In this paper the focus lies on machining with a twist-drill. Inside the drill are two coolant channels that supply the drilling process with cooling fluid, so the drilling hole is constantly filled with the fluid in order to reduce thermal loads. To further improve the cooling process, a novel drilling strategy is proposed, the discontinuous drilling. The central idea is to interrupt drilling during the process by retracting the tool from the contact zone, so that the coolant can flow around the cutting edge to transport the heat away from the contact zone, reducing thermal loads and tool wear. It is (nearly) impossible to reach the contact zone with measurement tools during the drilling process. So simulations are needed to further understand the discontinuous drilling strategy and to predict thermal loads for different sets of process parameters. The mathematical modeling of discontinuous drilling is non-trivial as several mathematical and numerical challenges arise. Firstly, the computational domain, the drilling hole with the tool, is highly rotational, an efficient and accurate description of the fluid domain is important. Secondly, the geometry of the drill (and the deformed chip) is rather complex. The simulation model must capture the geometry and (thermal) fluid-structure interaction (FSI) precisely. Finally, the whole discontinuous drilling process must be modeled, including the contact of the tool and workpiece as well as the interruptions. These mathematical challenges present the outline of this paper: first the fluid flow is modeled in a rotational domain. Next FSI is prescribed using the Fictitious Boundary Method (FBM). In the last section the discontinuous drilling is modeled by separating the contact and interruption configurations.

2 Fluidflow in a rotational frame of reference

Let $\boldsymbol{v}$ be the fluid velocity, p the pressure, ϱ the density and ν the viscosity of the coolant in a fluid domain Ω_f. The fluid flow is modeled with the incompressible Navier-Stokes equations

$$\begin{aligned} \varrho\frac{\partial \boldsymbol{v}}{\partial t} - \nu\Delta\boldsymbol{v} + (\boldsymbol{v}\cdot\nabla)\boldsymbol{v} + \nabla p &= \boldsymbol{f} \quad \text{in } \Omega_f \times (0,T) \\ \text{div } \boldsymbol{v} &= 0 \quad \text{in } \Omega_f \times (0,T) \end{aligned} \tag{1}$$

---

* Corresponding author: e-mail michael.fast@mathematik.tu-dortmund.de, phone +00 231 755 3177, fax +00 231 755 5933

on a given time interval $[0, T]$ with initial data for $t = 0$ and body forces $\boldsymbol{f}$. For sake of simplicity let the drill rotate around the z-axis with a constant velocity $\boldsymbol{\omega} := (0, 0, \omega)^\top$ with $\omega \in \mathbb{R}$. This means that the fluid domain is highly time dependent. To circumvent this problem, the equations (1) are transformed into a rotating frame of reference with the radius vector $\boldsymbol{r}$ and the transformed velocity $\boldsymbol{u} := \boldsymbol{v} + (\boldsymbol{\omega} \times \boldsymbol{r})$. Using the identity $\boldsymbol{\omega} \times (\boldsymbol{\omega} \times \boldsymbol{r}) = -\frac{1}{2}\nabla(\boldsymbol{\omega} \times \boldsymbol{r})^2$ the centrifugal forces $\boldsymbol{\omega} \times (\boldsymbol{\omega} \times \boldsymbol{r})$ can be included into the pressure with $P = p - \frac{1}{2}(\boldsymbol{\omega} \times \boldsymbol{r})^2$ and the Navier-Stokes equations in a rotational frame of reference become

$$
\begin{aligned}
\varrho\frac{\partial \boldsymbol{u}}{\partial t} - \nu\Delta\boldsymbol{u} + (\boldsymbol{u} \cdot \nabla)\boldsymbol{u} + 2\boldsymbol{\omega} \times \boldsymbol{u} + \nabla P &= \boldsymbol{f} &&\text{in } \Omega_f \times (0, T) \\
\operatorname{div} \boldsymbol{u} &= 0 &&\text{in } \Omega_f \times (0, T)
\end{aligned}
\tag{2}
$$

with Coriolis forces $2\boldsymbol{\omega} \times \boldsymbol{u}$. Details concerning the derivation and the analysis of equations (2) can be found in the literature [1].

2.1 Finite Element Discretization

The Navier-Stokes equations (2) in a rotational frame of reference are discretized in space with the Q2P1 Finite Elements and in time with the θ-scheme. Let the superscript $\{\cdot\}^n$ denote the quantity at timestep t_n with a timestep size $\Delta t := t_{n+1} - t_n$. The discrete equations than read

$$
\begin{aligned}
\varrho\frac{\boldsymbol{u}^{n+1} - \boldsymbol{u}^n}{\Delta t} + \theta\big((\boldsymbol{u}^* \cdot \nabla)\boldsymbol{u}^{n+1} - \nu\Delta\boldsymbol{u}^{n+1} + 2\boldsymbol{\omega} \times \boldsymbol{u}^{n+1}\big) + \nabla P^{n+1} &= \boldsymbol{rhs}^{n+1} &&\text{in } \Omega_f \times (0, T) \\
\operatorname{div} \boldsymbol{u}^{n+1} &= 0 &&\text{in } \Omega_f \times (0, T)
\end{aligned}
\tag{3}
$$

with right-hand side

$$
\boldsymbol{rhs}^{n+1} = \theta\boldsymbol{f}^{n+1} + (1 - \theta)\boldsymbol{f}^n - (1 - \theta)\big((\boldsymbol{u}^* \cdot \nabla)\boldsymbol{u}^n - \nu\Delta\boldsymbol{u}^n + 2\boldsymbol{\omega} \times \boldsymbol{u}^n\big)
$$

with a suitable approximation $\boldsymbol{u}^*$ of $\boldsymbol{u}^{n+1}$. Defining $N(\boldsymbol{u})$ and L as the discrete counterpart to the continuous operators $\boldsymbol{u} \cdot \nabla$ and Δ, respectively, the discrete gradient B and the mass matrix M, we get the discrete coupled equation of (3)

$$
\begin{pmatrix}
A & -2\Delta t\theta\omega M & 0 & \Delta tB_1 \\
2\Delta t\theta\omega M & A & 0 & \Delta tB_2 \\
0 & 0 & A & \Delta tB_3 \\
B_1^\top & B_2^\top & B_3^\top & 0
\end{pmatrix}
\begin{pmatrix}
\boldsymbol{u}_1 \\
\boldsymbol{u}_2 \\
\boldsymbol{u}_3 \\
\boldsymbol{p}
\end{pmatrix}
=
\begin{pmatrix}
\boldsymbol{rhs}_1^{n+1} \\
\boldsymbol{rhs}_2^{n+1} \\
\boldsymbol{rhs}_3^{n+1} \\
\boldsymbol{0}
\end{pmatrix}
\tag{4}
$$

with $A = M + \theta\Delta t(N(\boldsymbol{u}) + \nu L)$. For the sake of simplicity we set $B^\top = (B_1^\top\ B_2^\top\ B_3^\top)$, $\boldsymbol{rhs}^\top = (\boldsymbol{rhs}_1^{n+1\top}\ \boldsymbol{rhs}_2^{n+1\top}\ \boldsymbol{rhs}_3^{n+1\top})$ and

$$
S := \begin{pmatrix}
A & -2\Delta t\theta\omega M & 0 \\
2\Delta t\theta\omega M & A & 0 \\
0 & 0 & A
\end{pmatrix}
\tag{5}
$$

and hence we obtain the saddlepoint problem

$$
\begin{pmatrix}
S & B \\
B^\top & 0
\end{pmatrix}
\begin{pmatrix}
\boldsymbol{u} \\
\boldsymbol{p}
\end{pmatrix}
=
\begin{pmatrix}
\boldsymbol{rhs} \\
\boldsymbol{0}
\end{pmatrix}.
\tag{6}
$$

The numerical method to solve the systems of equations (6) and modifications to take the Coriolis forces into account will be discussed in the following section.

2.2 Discrete Projection Method

The discrete saddlepoint problem (6) is solved with the Discrete Projection Method (DPM) which consists of three steps for each timestep as depicted in algorithm 1. To get an initial prediction for the velocity, the viscous Burgers equation for an intermediate velocity $\bar{\boldsymbol{u}}$ is solved in the first step. In the second step the Pressure Poisson (PP) problem is solved with the PP matrix $B^\top C^{-1}B$ and the discrete divergence of $\bar{\boldsymbol{u}}$ as right-hand side. The matrix C is an appropriate preconditioner to S and should be a good approximation and its inverse must be computationally cheap. In a final step the velocity and pressure are corrected for the next timestep or fixpoint iteration. The resulting systems of equations is each solved with a geometric multigrid solver [3]. Further details concerning DPM can be found in [2]. The choice of C is crucial for the efficiency of algorithm 1. For small timesteps sizes, $C = M_l$ is a good approximation for S, as it is the case for the drilling application. However, Coriolis forces are not taken into account, so they are added to get

$$
M_{coriolis} := \begin{pmatrix}
M_l & -2\omega\Delta t\theta M_l & 0 \\
2\omega\Delta t\theta M_l & M_l & 0 \\
0 & 0 & M_l
\end{pmatrix}.
\tag{7}
$$

Algorithm 1 Discrete Projection Method (DPM)

1. Solve the viscous Burgers equation for the intermediate solution $\bar{\boldsymbol{u}}$

$$S(\boldsymbol{u}^n)\bar{\boldsymbol{u}} = \boldsymbol{rhs} - \theta \Delta t B \boldsymbol{p}^n$$

2. Solve the Pressure Poisson problem for the intermediate solution $\boldsymbol{q}$

$$B^\top C^{-1} B \boldsymbol{q} = \frac{1}{\Delta t} B^\top \bar{\boldsymbol{u}}$$

3. Correction of the pressure and velocity

$$\begin{aligned}
\boldsymbol{p}^{n+1} &= \boldsymbol{p}^n + \boldsymbol{q} + \alpha M_{\boldsymbol{p}}^{-1} B^\top \bar{\boldsymbol{u}} \\
\boldsymbol{u}^{n+1} &= \bar{\boldsymbol{u}} - \Delta t C^{-1} B \boldsymbol{q}
\end{aligned}$$

Due to the block diagonal structure of (7) its inverse is explicitly given by

$$M_{coriolis}^{-1} := \frac{1}{(1 + [2\omega\Delta t\theta]^2)} \begin{pmatrix} M_l^{-1} & 2\omega\Delta t\theta M_l^{-1} & 0 \\ -2\omega\Delta t\theta M_l^{-1} & M_l^{-1} & 0 \\ 0 & 0 & (1 + [2\omega\Delta t\theta]^2)M_l^{-1} \end{pmatrix}. \tag{8}$$

The resulting PP matrix $B^\top M_{coriolis}^{-1} B$ is asymmetrical for Q2P1 Finite Elements. In order to overcome this problem, the symmetric part $M_{sym}^{-1} := \frac{1}{2}\left(M_{coriolis}^{-1} + M_{coriolis}^{-\top}\right)$ of $M_{coriolis}^{-1}$ is considered. This preconditioner reproduces the property $(\nabla \cdot \mathcal{M}_{coriolis}^{-1} \nabla)_{asymmetric} \equiv 0$ with the continuous Coriolis mass matrix $\mathcal{M}_{coriolis}$, so M_{sym}^{-1} is a good approximation to the continuous operators.

3 Geometrical modeling of the drilling process

The transformation into a rotating frame of reference as described in section 2 enables the modeling of the drill as a static obstacle embedded in the fluid domain. Consequently only one computational grid for all timesteps has to be constructed so the geometry of the tool can be captured accurately. This will be done with a combination of the Fictitious Boundary Method (FBM) and a mesh deformation technique, which will be the focus in this section.

3.1 Fictitious Boundary Method

FBM is a filtering technique to decompose the computational domain into its solid part Ω_s and fluid part Ω_f respectively. Based on a surface representation of the tool, a signed distance function d with $d(\boldsymbol{x}) > 0$ for $\boldsymbol{x} \in \Omega_f$ and $d(\boldsymbol{x}) < 0$ for $\boldsymbol{x} \in \Omega_s$ is calculated. The solid-fluid interface is given by $d(\boldsymbol{x}) = 0$. With this distance function an indicator function

$$\alpha(\boldsymbol{x}) := \begin{cases} 1, & \boldsymbol{x} \in \Omega_s \\ 0, & \boldsymbol{x} \in \Omega_f \end{cases} \tag{9}$$

can be defined. Internal boundary conditions as well as material parameters are set according to the values of α. The major advantage of FBM is that only one mesh for Ω_s and Ω_f is constructed and the interactions between the solid and the fluid are modeled implicitly with the internal boundary conditions. Details concerning FBM can be found in [4]. For this the mesh must capture the fluid-solid interface accurately, which will be achieved with mesh deformation.

3.2 Mesh Deformation

Starting from a structured mesh, the goal is to determine a mesh size distribution without changing the connectivity of the underlining grid. With a user defined monitor function $\mathfrak{M}$ weights w_i are calculated that control the mesh size density. For an precise representation of the tool surface the signed distance function as described in section 3.1 is a straightforward choice. With Algorithm 2 the mesh nodes are moved according to the calculated weights w_i in an iterative fashion with a relaxation parameter τ. An exemplary depiction of the the deformed mesh based on the signed distance function corresponding to a surface representation of the tool can be found in figure 1. Algorithm 2 is purely algebraic, so no further partial differential equations have to be solved.

Algorithm 2 Algebraic mesh deformation

For given weights w_i, edges e_{ij} and node coordinates $\boldsymbol{x}_i$ calculate the new coordinates

for $i = 1, \dots, n$ do

$$\boldsymbol{x}_i^{new} = (1-\tau)\boldsymbol{x}_i^{old} + \tau \left(\sum_{j=1,n}^{\text{if } \exists e_{ij}} w_j \boldsymbol{x}_j^{old} \right) \left(\sum_{j=1,n}^{\text{if } \exists e_{ij}} w_j \right)^{-1}$$
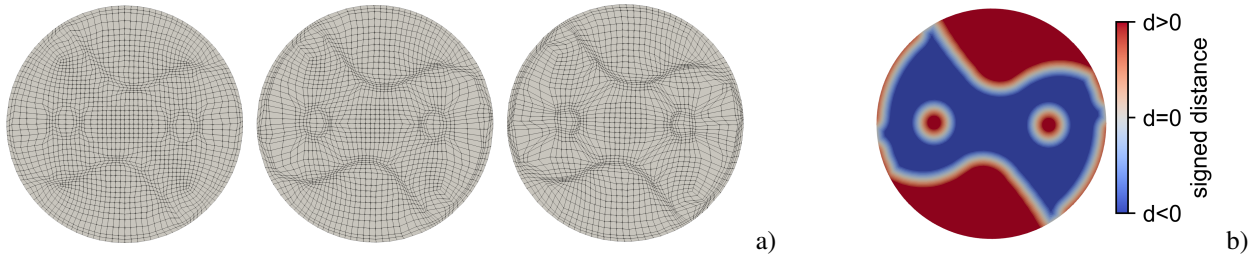
end do

with a relaxation parameter $\tau \in (0, 1]$.

Fig. 1: Mesh deformation (a) based on calculated signed distance function (b)

4 Discontinuous drilling simulation model

In order to model the discontinuous drilling process, the simulation is decomposed into a 'No Contact' (NC) and a 'Contact' (C) configuration. Both configurations are simulated separately and coupling makes use of FBM. One grid is constructed for both settings and simply by switching the α values corresponding to the workpiece at the borehole ground. So first a simulation model for each configuration has to established before the discontinuous drilling model is constructed. For the following numerical examples in this section the process and material parameters as depicted in table 1 are used.

Processparameters	Coolant	Workpiece	Tool
$\dot{Q}$: 3.3 l/min	ϱ : 0.85 g/cm^3	ϱ : 8.19 g/cm^3	ϱ : 14.45 g/cm^3
U : 995 min^{-1}	c_p : 2.02 $J/(g \cdot K)$	c_p : 0.45 $J/(g \cdot K)$	c_p : 0.2 $J/(g \cdot K)$
h : 70 kW	λ : 0.00139 $W/(cm \cdot K)$	λ : 0.095 $W/(cm \cdot K)$	λ : 0.86 $W/(cm \cdot K)$
	ν : 0.02 $Pa \cdot s$		

Table 1: Process and material parameters of coolant, Inconel 718 and tool

4.1 Simulation model for 'No Contact' and 'Contact' configuration

The simulation algorithm for the 'No Contact' and 'Contact' configuration decouples the Navier-Stokes equations for the fluid flow and the heat equation. After a preprocessing step a fully developed velocity field is calculated as a representative for the fluid flow for a set of process and geometry data. This velocity field is then used for the simulation of the cooling process. With FBM the heat equation is solved in $\Omega = \Omega_s \cup \Omega_f$ on a unified mesh for the solid and fluid domain. The outline for the model is summarized in algorithm 3.

First the simulated flow field is validated for the 'No Contact' configuration for a different set of distances of the tool to the workpiece and inflow velocities. The calculated velocities are compared with the corresponding experimental setup using the Particle Tracking Velocimetry (PTV). The results that can be seen in [5] show good agreement of the simulation to the experiments.

Next the heating during the 'Contact' configuration is simulated with algorithm 3 using a fictional heat source at the cutting edge, where the tool geometry intersects the workpiece geometry, and an initial calculated velocity field. For now the geometry of the deformed chip is neglected. The result that will act as comparison to the discontinuous setup is depicted in figure 2. As can be seen in figure 2, the temperature increases continuously until some saturation is reached as expected. Also the temperature distribution on the tool surface is depicted. In the following section this result will be compared to the results of the discontinuous drilling simulation.

4.2 Coupling of 'No Contact' and 'Contact' configuration

The central idea of the discontinuous drilling simulation model is to calculate the 'No Contact' and 'Contact' configurations on the same grid using again the possibilities of FBM. Coupling of both configuration is done by switching the properties of

---

Algorithm 3 Simulation model for 'No Contact' and 'Contact' configuration

1. Preprocessing (FBM, Material assignment, Boundary Conditions, ...)

2. **while** not (Fluid flow fully developed) **do**

   Solve Navier-Stokes equations in Ω_f

   end while

3. **while** ($t \leq T$) **do**

   Solve heat equation in Ω_f and Ω_s

   end while

4. Postprocessing
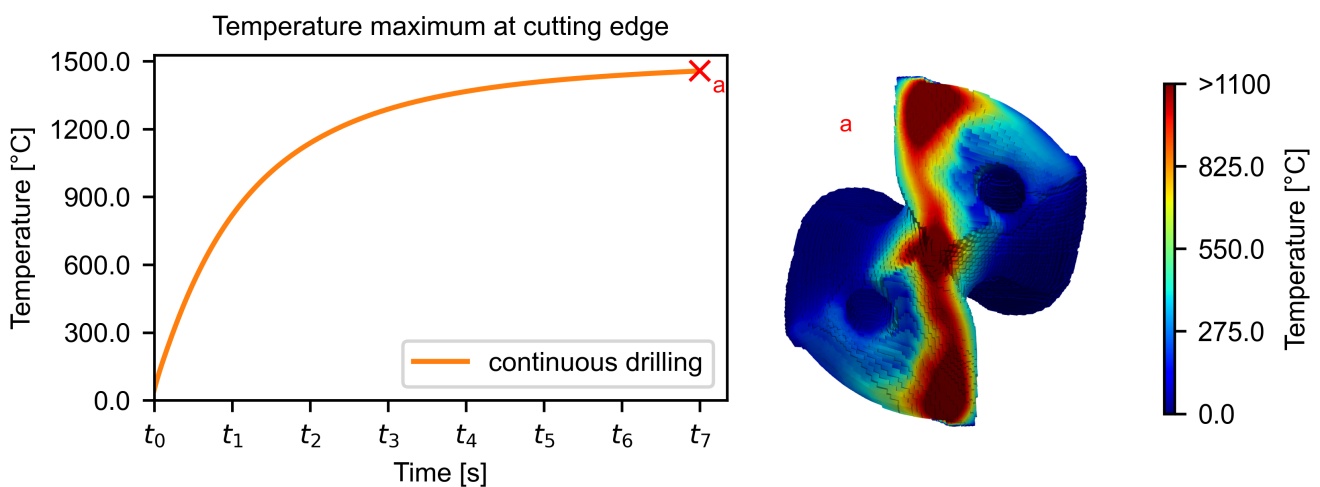
Fig. 2: Conceptional simulation of heating process during conventional drilling with coolant flow

the elements that correspond to the workpiece. This enables the simulation to change the configuration during the retraction of the tool flexibly and no remeshing or data transfer is needed. The outline for this model is presented in algorithm 4. For the sake of simplicity, the retraction movement of the tool between these configurations is neglected. The influence of this part of the process, and the possible suction that might occur, has to be investigated in future work. A representative flow field is

---

Algorithm 4 Discontinuous drilling simulation model

1. Preprocessing for (C) and (NC) on the <u>same</u> grid

2. **while** not (Fluid flow fully developed) **do**

   Solve Navier-Stokes equations for (C) and (NC) in Ω_f

   end while

3. **for all** cycles **do**

   Get velocity field from current configuration

4. **while** $t \leq T_{cycle}$ **do**

   Solve heat equation in Ω_f and Ω_s

   end while

5. Transfer temperature field to next configuration

6. Postprocessing

---

calculated for both configurations. Alternating between the configurations and setting the heat source on or off in accordance with the configuration, starting with the 'Contact' configuration, the corresponding velocity field is set and the temperature equation is solved until some time T_{cycle}. The temperature field at T_{cycle} is set as initial temperature for the next configuration. The resulting temperatures for the same setup as in section 4.1 and with equally distributed interruptions over time are depicted in figure 3. In figure 3 it can be seen that the temperature has a seesaw shape, as expected, so the temperature increases during
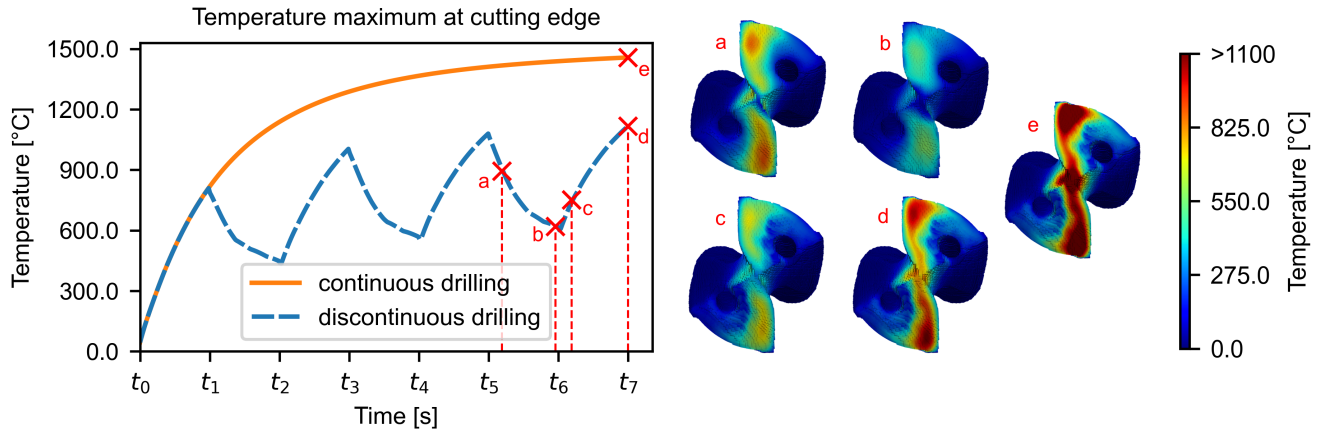

Fig. 3: Conceptional simulation of heating process during the discontinuous drilling with coolant flow and comparison to continuous drilling

the 'Contact' time intervals and again decreases in the 'No Contact' intervals. In comparison to the continuous drilling setup the overall temperatures decrease significantly which indicates that tool wear can be reduced with the discontinuous drilling strategy. This can also be observed in the temperature distribution on the cutting edges. The coolant successfully transports the heat out of the contact zone during the retractions of the tool reducing the thermal loads on the cutting edge.

5   Outlook

Further improvements to the presented simulation model of the discontinuous drilling strategy will focus on the accuracy of the model concerning the fluid, thermal loads, and the geometry. For now the fluid is treated as Newtonian albeit initial investigations show that the viscosity is temperature dependent so modifications to the Navier-Stokes solver has to be made to take non-Newtonian fluids into account. DEFORM [6] simulations will be used to get accurate initial temperature data, heat sources due to chip formation and initial temperature field for the CFD simulation. Additionally the resulting chip geometry calculated with DEFORM will be included in the CFD simulation. With an accurate and flexible simulation model at hand the sensitivity of the process with respect to different process parameters can be analyzed in order to find an optimal set of process parameters.

References

[1] A. Sokolov, S. Turek, M. Olshanskii, Numerical study of a new discrecte projection method for rotating incompressible flows, Electronic Transactions on Numerical Analysis **32**, 49–62 (2008).
[2] S. Turek, On discrete projection methods for the incompressible Navier–Stokes equations: An algorithmical approach, Computer Methods in Applied Mechanics and Engineering **143**, 271–288 (1997).
[3] S. Turek, Efficient Solvers for Incompressible Flow Problems: An Algorithmic and Computational Approach (Springer Science & Business Media, 1999).
[4] R. Münster, O. Mierka, S. Turek, Finite element-fictitious boundary methods (FEM-FBM) for 3D particulate flow, International Journal for Numerical Methods in Fluids **69**, 294–313 (2012).
[5] T. Wolf, M. Fast, D. Biermann, S. Turek, Particle Tracking Velocimetry in high-speed analysis of coolant flow to validate a numerical model concerning discontinuous drilling of the nickel-base alloy Inconel 718, 16th CIRP Conference on Intelligent Computation in Manufacturing Engineering, CIRP ICME '22, Gulf of Naples, 13-15 July 2022.
[6] https://www.deform.com/